

# RELEVANT METHODOLOGIES FOR THE CHARACTERIZATION OF IRRADIATED MATERIALS

**Cornelia Vasile<sup>1/</sup>, Elena Stoleru<sup>1/</sup>, Sossio Cimmino<sup>2/</sup>, Clara Silvestre<sup>2/</sup>**

*<sup>1/</sup> “Petru Poni” Institute of Macromolecular Chemistry, Physical Chemistry of Polymers Department, Romanian Academy, 41A Grigore Ghica Voda Alley, 700487 Iasi, Romania*

*<sup>2/</sup> Istituto per i Polimeri, Compositi e Biomateriali, Consiglio Nazionale delle Ricerche, IPCB/CNR, Via Campi Flegrei 34, 80078 Pozzuoli, Naples, Italy*

## 1. INTRODUCTION

Irradiation dose and dose rate affect either the surface properties only and/or the bulk properties of a material as well. Dose and dose rate should be established according to the final end use of the material being irradiated. The bulk and surface properties of polymers differ in terms of the chemical structure, the morphology and the surface energy because of the oxidation of surfaces and the orientation of macromolecules in a way that can enhance their interactions [1].

## 2. METHODOLOGIES FOR THE CHARACTERIZATION OF SURFACE PROPERTIES

Surface properties play an important role in a number of applications where polymeric materials are used. A property, such as surface wetting, is important in printing and in adhesive bonding and in the manufacture of membranes and biomedical devices [2, 3]. The covalent bonds of polymers and the mobility of polymeric chains lead to the unique effects on the surface properties of polymers. Surface layers display compositions and properties that are time-dependent and can vary with the conditions to which a polymer is exposed. When a polymer is in contact with a solid substrate, the polymer molecular mobility leads to important differences. The number of chemical elements found in

Table 1. Summary of surface analysis techniques. (Adapted from Ref. [4]).

Direct surface analysis methods			
Incident excitation by	Emitted analyzed response		
	Electrons	Ions	Photons
Electrons	<ul style="list-style-type: none"> <li>- Auger electron spectroscopy (AES)<sup>a</sup></li> <li>- Scanning Auger microscopy (SAM)<sup>a</sup></li> <li>- Scanning electron microscopy (SEM)<sup>a</sup></li> <li>- Transmission electron microscopy (TEM)<sup>a,b</sup></li> <li>- Low energy electron diffraction (LEED)<sup>a</sup></li> <li>- Reflection high energy electron diffraction (RHEED)<sup>a</sup></li> <li>- Spin polarized electron spectroscopy (SPE)<sup>a,b</sup></li> </ul>		<ul style="list-style-type: none"> <li>- Energy dispersive analysis of X-rays (EDAX)<sup>b</sup></li> </ul>
Ions		<ul style="list-style-type: none"> <li>- Secondary ion mass spectrometry (SIMS)<sup>a</sup></li> <li>- Low energy ion scattering spectroscopy (LEIS)<sup>a</sup></li> <li>- Rutherford backscattering spectroscopy (RBS)<sup>b</sup></li> </ul>	<ul style="list-style-type: none"> <li>- Nuclear reaction analysis (NRA)<sup>b</sup></li> </ul>
Photons	<ul style="list-style-type: none"> <li>- X-ray photoelectron spectroscopy/electron spectroscopy for chemical analysis (XPS/ESCA)<sup>a</sup></li> <li>- Ultraviolet photoelectron spectroscopy (UPS)<sup>a</sup></li> <li>- Auger emission extended X-ray absorption fine structure ((AE)XAFS)<sup>a</sup></li> </ul>		<ul style="list-style-type: none"> <li>- Fourier transform infrared spectroscopy (FTIR)<sup>b</sup></li> <li>- Raman vibrational spectroscopy (Raman)<sup>b</sup></li> <li>- X-ray absorption fine structure analysis (XAFS)<sup>b</sup></li> </ul>
Electric/magnetic field	<ul style="list-style-type: none"> <li>- Scanning tunneling microscopy (STM)<sup>a</sup></li> <li>- Atomic force microscopy (AFM)<sup>a</sup></li> </ul>		<ul style="list-style-type: none"> <li>- Glow discharge optical emission spectroscopy (GDOES)<sup>a</sup></li> </ul>

<sup>a</sup> Surface < 10 nm.<sup>b</sup> Near surface ~1 µm.

polymers is quite limited, with C, H, N, O and Si and sometimes F, Cl, Br, and S, but the way in which these elements can be assembled into polymeric materials is unlimited.

The important properties of polymer surfaces are: surface composition, free surface energy, wettability, roughness, zeta potential, polymer surface dynamics, aging behavior, wetting transition, adhesion, barrier properties, friction and wear, biocompatibility, bioadhesion, *etc.* Methods to determine these properties are listed in Table 1. The properties of polymers depend on the average molecular weight, crosslinked density and processing conditions.

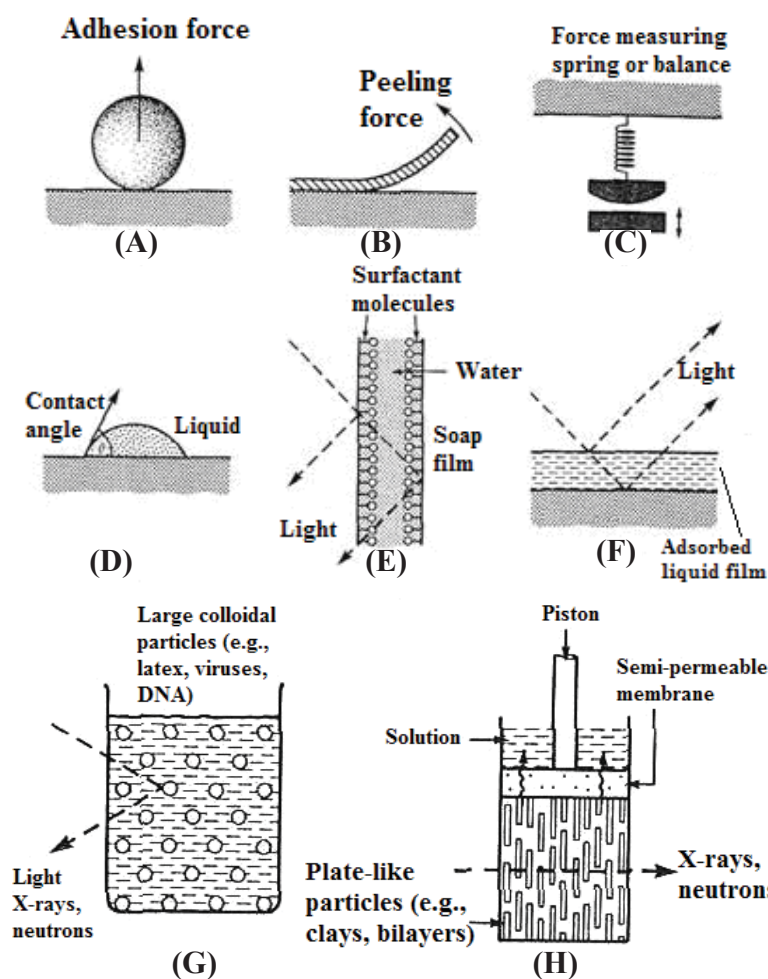


Fig.1. Schematic representation of the measurement of forces between particles and surfaces: (A) adhesion measurements, (B) peeling measurements, (C) direct measurement of a force as a function of surface separation, (D) contact angle measurement, (E) equilibrium thickness of thin free films (soap films, foams), (F) equilibrium thickness of thin adsorbed film, (G) interparticle spacing in liquids (colloidal suspensions, paints, pharmaceutical dispersions), (H) sheet-like particle spacing in liquids. (Adapted from Ref. [5]).

Table 2. Comparison between the possibilities offered by the analysis techniques in the study of polymer surfaces [6, 7].

Technique	Depth resolution	Lateral resolution	Depth profiling	Imaging & mapping	Quantitative accuracy	Detection limits/sensitivity	Sample considerations	
XPS/ESCA	5 to 30 nm	> 250 $\mu\text{m}$	Ion-etching, angle-resolved	None	5%	0.1 monolayer 0.1 at% $Z > 2/10^{-2}-10^{-3}$	Ultra-high vacuum	
AES/SAM	2 to 30 nm	> 30 nm	Ion-etching, angle-resolved	SEM elemental & chemical	20%	0.1 monolayer 0.1 at% $Z > 2$	Ultra-high vacuum, electron beam (EB), damage, charging	
FTIR	ZnSE-ATR: 2-4 $\mu\text{m}$ , GE-ATR: 0.4-1 $\mu\text{m}$	10 $\mu\text{m}$	See ATR	No	Low % (solution)	ng $\mu\text{g}/10^{-2}$	Yes	
Raman	5 $\mu\text{m}$	1 $\mu\text{m}$	Limited	Yes	No	$\mu\text{g}/10^{-1}-10^{-2}$	Yes	
EDS	$\sim 1 \mu\text{m}$	$\sim 1 \mu\text{m}$	No	SEM elemental line-scans	5%	10 ppm $Z > 5$	High vacuum, electron beam damage	
Topographic probes								
Technique	Lateral		Vertical		Sample considerations			Additional capabilities
	Resolution	Range	Resolution	Range				
SEM	3 nm	N/A	N/A	N/A	High vacuum, electron beam damage			Backscatter mode
AFM/STM	< 0.1 nm	100 $\mu\text{m}$	< 0.1 nm	7 $\mu\text{m}$	Air or liquid, < 25 mm diameter, < 10 mm high			Lateral force, nanoindentation
Nanoindentation	< 100 nm	300 $\mu\text{m}$	< 100 nm	500 $\mu\text{m}$	Samples with a homogeneous microstructure			

Indirect methods for surface investigation are the following: contact angle methods, atomic force microscopy (AFM), differential thermal analysis (DTA), differential scanning calorimetry (DSC), molecular mass distribution, nanoindentation, *etc.*

The methods used to determine specific surface properties are:

- composition: AES/SAM, XPS (X-ray photoelectron spectroscopy), SEM/EDS (scanning electron microscopy/energy-dispersive), SIMS (secondary ion mass spectrometry);
- chemistry: XPS, FTIR/Raman, SIMS;
- morphology/topography: SEM, AFM/STM, nanoindentation.

The principles of several types of measurements are schematically represented in Fig. 1.

Particle detachment (Fig. 1A) and peeling forces (Fig. 1B) provide information on adhesion forces that are attractive forces when solid surfaces are in contact. Figure 1B is a peel test, which has practical use when evaluating adhesive tapes, material fracture and crack propagation. A spring or a balance can be used to measure the separation force between two macroscopic surfaces as a function of the separation distance (Fig. 1C). Surface tension and contact angle measurements give information on liquid-liquid or liquid-solid surface contact (Fig. 1D). This is used for testing wettability and the stability of surface films, and detergency. The thickness of free soap films and liquid films adsorbed on surfaces (Figs. 1E and F) can be measured and this gives information on the repulsive forces that stabilize wetting films. Optical techniques, as internal reflection spectroscopy or ellipsometry, are used to measure film thickness of about 0.1 nm. Dynamic interparticles separation and motions in liquids can be measured by nuclear magnetic resonance (NMR), light scattering, X-ray scattering and neutron scattering (Fig. 1G). Sheet-like (lipid bilayers) or rod-like particles are examined applying methods, as illustrated in Figs. 1G and H. This last method is useful in studying the microstructure of soaps and of biological membranes.

Depending on the measurement principle, each method has some limits wherein it can be used (Table 2).

## 2.1. DEPTH PROFILING TECHNIQUES

Depth profiling is used to determine the composition of one or more components of a film as a function of depth.

Secondary ion mass spectroscopy (SIMS) (Fig. 2) operates on the principle that bombardment of a material with a high energy ion beam (primary ions) results in the ejection or sputtering of atoms from the material [10, 11]. In SIMS analyses, material is removed from the sample by sputtering, and is, therefore, a locally destructive technique.

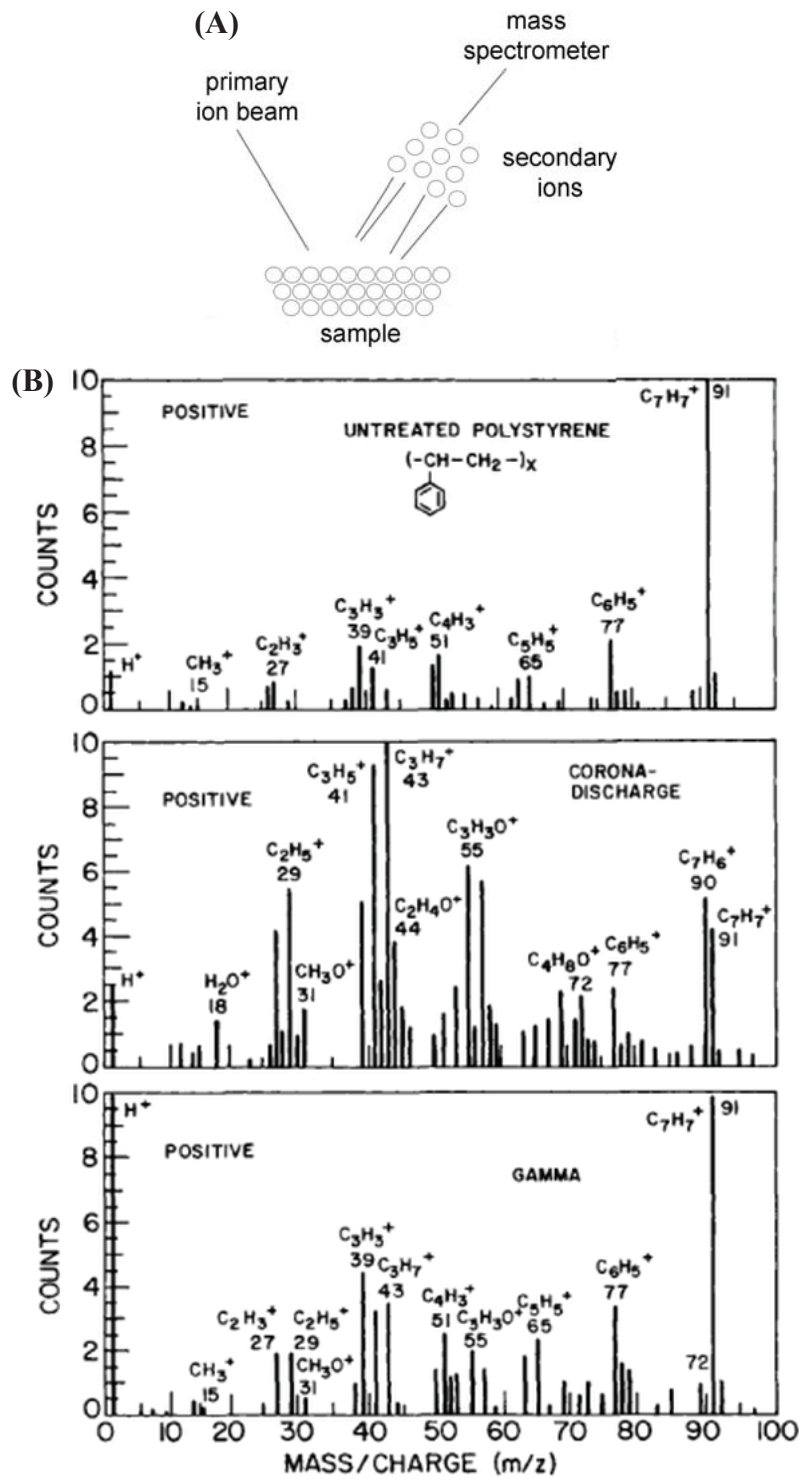


Fig.2. The principle of SIMS (A), positive static SIMS spectra for unirradiated and irradiated polystyrene (B) [8, 9].

In static SIMS, the primary ion fluence must be kept low enough ( $< 10^{13}$  ions $\cdot$ cm $^{-2}$ ) to prevent a surface area from being hit more than once. For this reason, this technique is considered as non-destructive.

Dynamic SIMS is widely used to analyze thin films, layer structures and dopant profiles.

Time of flight-secondary ion mass spectrometry (ToF-SIMS) uses principles very similar to SIMS, but removes a very small amount of material from the sample as compared to the relatively large amount removed by SIMS analysis. ToF-SIMS identifies elements and bonding states of atoms present on the very surface of a sample, the outer one or two monolayers. It is used for depth profiling of various organic and inorganic films, including polymer films and multilayer films and film fragments. The emitted ions are related to the chemical structure of the materials and usually consist of molecular and quasi-molecular ions that occur from fragmentation, rearrangement, decomposition and reaction of the constituent molecules of the material.

SIMS is an excellent tool for surface analysis because of its many advantages, such as: (i) the detection of large organic molecules up to several thousands of mass units, (ii) fast data acquisition with a time of flight (ToF) analyzer; and (iii) chemical information on the top few angstroms layers of material is obtained. SIMS imaging is one of the exciting developments in this field.

Monitoring secondary ion emission in relation to sputtering time allows for depth profiling of the sample composition. Layers of up to 10 000 Å thick can be depth-profiled using SIMS. SIMS can provide an accuracy of about 6% and a precision of less than 0.5%.

Analytical information obtained using SIMS are the following:

- Mass spectrum – identifies the elemental and ion composition of the uppermost 10 to 20 Å of the analyzed surface.
- Depth profile – under typical static SIMS conditions (2 keV < ion energy < 4 keV), the primary ions penetrate to a depth of ~3 nm below the surface. A depth resolution of a few angstroms is possible.
- Secondary ion mapping – measures the lateral distribution of elements and molecules on the surface. Lateral resolution is less than 100 nm for elements and about 500 nm for large molecules.

Libraries of static SIMS spectra [12] provide a guide for the interpretation of results. Careful spectral interpretation combined with fragmentation pathways (*e.g.* on pyrolysis/electron impact mass spectrometry) allows different classes of polymers to be distinguished as well as individual members of one class to be identified. The complementary combination of XPS and static SIMS is a powerful tool in the surface analysis of modified polymers [8].

Gamma irradiation of polystyrene (PS) to 150 kGy leads to surface oxidation of the polymer to depths greater than 10 nm as opposed to  $\approx 3$  nm depth attained by either plasma or corona-discharge treatment. Peaks indicative of the presence of aliphatic oxygen containing molecular ions were also observed.



The data suggests that oxidation by corona discharge is restricted to the top monolayers of the surface within the SIMS sampling depth ( $\sim 3$  nm). With gamma irradiation, the oxidized layer is considerably deeper into the bulk of the polymer [9].

ATR-FTIR and Raman spectroscopy non-destructively identify molecular species through their vibration states, chemical bond information and molecular orientation. Very little sample preparation is necessary. An attenuated total reflection (ATR) accessory operates by measuring the changes that occur in a totally internally reflected infrared beam when the beam comes into contact with a sample (Fig.3A). ATR-FTIR spectroscopy reflects more than just the outermost atomic layers, generally from 1000 Å up to 1 µm; but generally, penetration depth ranges from 40 Å to 3 µm.

For ATR-FTIR to be successful, the following two requirements must be met: (i) the sample must be in direct contact with the ATR crystal, because the evanescent wave or bubble only extends beyond the crystal from 0.5 to 5 µm; (ii) the refractive index of the crystal must be significantly greater than that of the sample, if not, internal reflectance will not occur. The most popular ATR crystal materials are zinc selenide (ZnSe), germanium and diamond which, because of its robustness, is often preferred.

Using the ATR-FTIR method, Gupta *et al.* had studied the effect of gamma irradiation on CR-39 polymer ( $C_{12}H_{18}O_7$ )<sub>n</sub> (which is a nuclear track detector and is used in optical devices) [14]. Parparita *et al.* had studied gamma irradiation induced changes on polypropylene (PP) biocomposites containing different bio-additives (Fig.3C) [13]. The results of Gupta *et al.* [14] study clearly indicated the lowering of the thermal stability of CR-39 as an effect of gamma irradiation, as shown in Fig.3B.

The gamma irradiation of PP and PP/biomass composites resulted in the formation of hydroxyl (mainly hydroperoxides and alcohols) ( $3350\text{ cm}^{-1}$ ) and carbonyl groups (mainly ketones, esters and acids) ( $1740\text{ cm}^{-1}$ ) which were detected by infrared spectroscopy [13] in the 3200-3600 and 1900-1500  $\text{cm}^{-1}$  region, respectively. The carbonyl and hydroxyl indices increased with the absorbed dose (Fig.3C). It was stated that these changes could be related either to polymer oxidation or to a higher content of biomass found at composite surfaces after irradiation.

X-ray photoelectron spectroscopy (XPS) is perhaps the most widely used surface spectroscopy and one of the more popular spectroscopic techniques available for the surface characterization of polymers [15, 16]. Samples irradiated with X-rays emit photoelectrons which characterize the binding energies (BE) of the elements in the sample and the chemical bonding of those elements. The photoemission peaks in the XPS spectra allow identification of all elements except hydrogen and helium. Monoenergetic soft X-rays (usually  $AlK_{\alpha}$  or  $MgK_{\alpha}$ ) are used to irradiate a sample material in high vacuum (typically  $\leq 10^{-9}$  torr). The emitted photoelectrons are collected with an electron lens assembly and



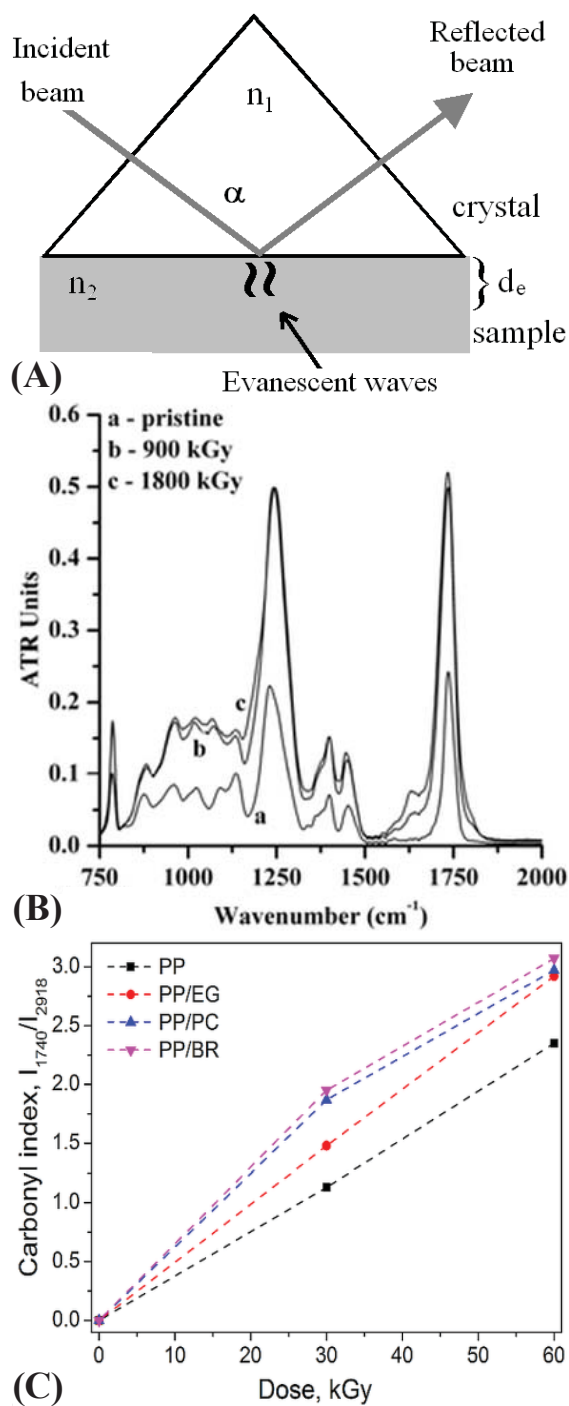


Fig.3. (A) Scheme of ATR-FTIR principle; (B) ATR-FTIR spectra of pristine CR-39 polymer unirradiated and gamma-irradiated to different doses; (C) dose-dependent variations of carbonyl index in irradiated PP and in different PP/biomass composites: PP/*Eucalyptus globulus* (EG), PP/*pine cones* (PC), PP/*Brassica Rapa* (BR) [13].

their energy is analyzed and counted. Since the energy levels in materials are quantified, the resulting energy spectrum consists of discrete peaks associated to the electronic energy states in the sample. The peaks of a photoelectron spectrum are grouped in three categories: (i) peaks due to photoemission from the core levels of the atom, (ii) those due to photoemission from the valence level and (iii) those due to Auger emission.

Analysis of the core level binding energies (*i.e.* measurement of chemical electron shifts) and of core level intensities, use of shake-up satellites, depth profiles and spatially resolved studies, and finally valence band spectra, are shown to produce many different but complementary keys to obtain information about the atomic, chemical and structural composition of macromolecular surfaces. The XPS emission process is represented schematically in Fig.4. Absolute binding energies (BE) of an emitted photoelectron are the energy difference between  $(n - 1)$ -electron final state ( $E_f$ ) and the  $n$ -electron initial state ( $E_i$ ) in the atom:

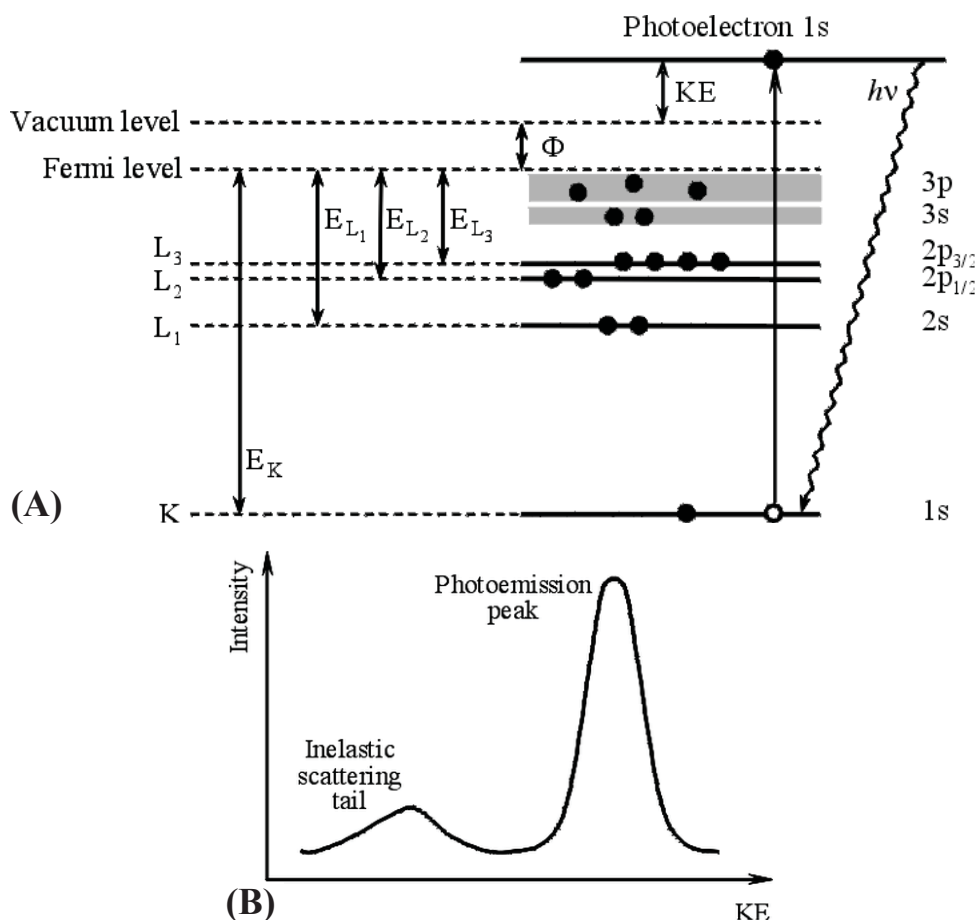


Fig.4. XPS photoemission process (A) and characteristic shape of a photoelectron peak, with contribution from the inelastic scattering background (B).

$$BE = E_f(n-1) - E_i(n) \quad (1)$$

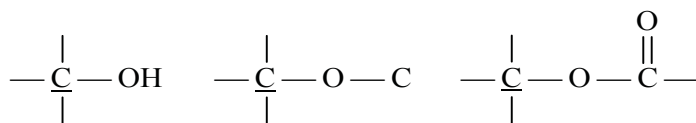
BE can be obtained by measuring the kinetic energy of the photoelectrons. The identification of the elements present on the surface is done directly by determining the binding energies of the core photoelectrons.

For energetic (950-1200 eV) electrons, XPS spectrometry ( $AlK_{\alpha}$  X-ray source) provides an evaluation of the C1s, N1s, and O1s levels (most common core levels encountered in polymers) by varying the take-off measurement angle from  $\sim 10$ - $90^\circ$ , which corresponds to the analysis in depth from  $\sim 1$  to 10 nm. The change in binding energy is known as the chemical shift. The chemical shift is closely related to the electronegativity of the species to which the atom of interest is bonded, which makes possible the chemical analysis of a given sample. Chemical shifts can range from a few tenths of an eV up to  $\sim 8$  eV. The C1s BE increases monotonically with the number of oxygen atoms bonded to carbon, that is  $C-C < C-O < C=O < O-C=O < O-(C=O) O-$ . Consistent with this, the carbon becomes more positive. The reference photoemission peak in polymer XPS spectra is the C1s line (285.0 eV) from a hydrocarbon chain ( $\underline{C}-C$ ,  $\underline{C}-H$ ). Typical C1s, O1s, *etc.* binding energies for covalent bonds are tabulated and provided in Ref. [17].

The XPS intensity (the integrated area under the photoelectron peak) is proportional to the atom quantity. Therefore quantitative elemental analysis of the material can be made. In most cases, the deconvolution of complex experimental peaks is necessary. Standard samples are poly(tetrafluoroethylene) (C and F) and polyethylene glycol (C and O).

Core level information are as follows:

- Shake-up peaks (also called loss peaks because intensity is lost from the primary photoemission peak) are most apparent for systems with aromatic structures, unsaturated bonds or transition metal ions.
- Surface derivatization technique has been developed, as a complementary method, to determine the density of specific species on treated surfaces. This method allows for precise identification of chemical groups, using a chemical reaction specific to only the functional group of interest. For example, examining substances containing functional groups like those below:



Peaks due to these groups in C1s spectra exhibit almost equal binding energies (about 286.5 eV) and, hence, cannot be separated using mathematical procedures, making the derivatization technique absolutely necessary. After treatment of a surface of non-polar polymers such as polyethylene (PE) and polypropylene by flame or plasma, with the objective to incorporate oxygen at the surface in order to improve adhesive properties, it is not possible to discriminate an ether from an epoxide or an alcohol structure,

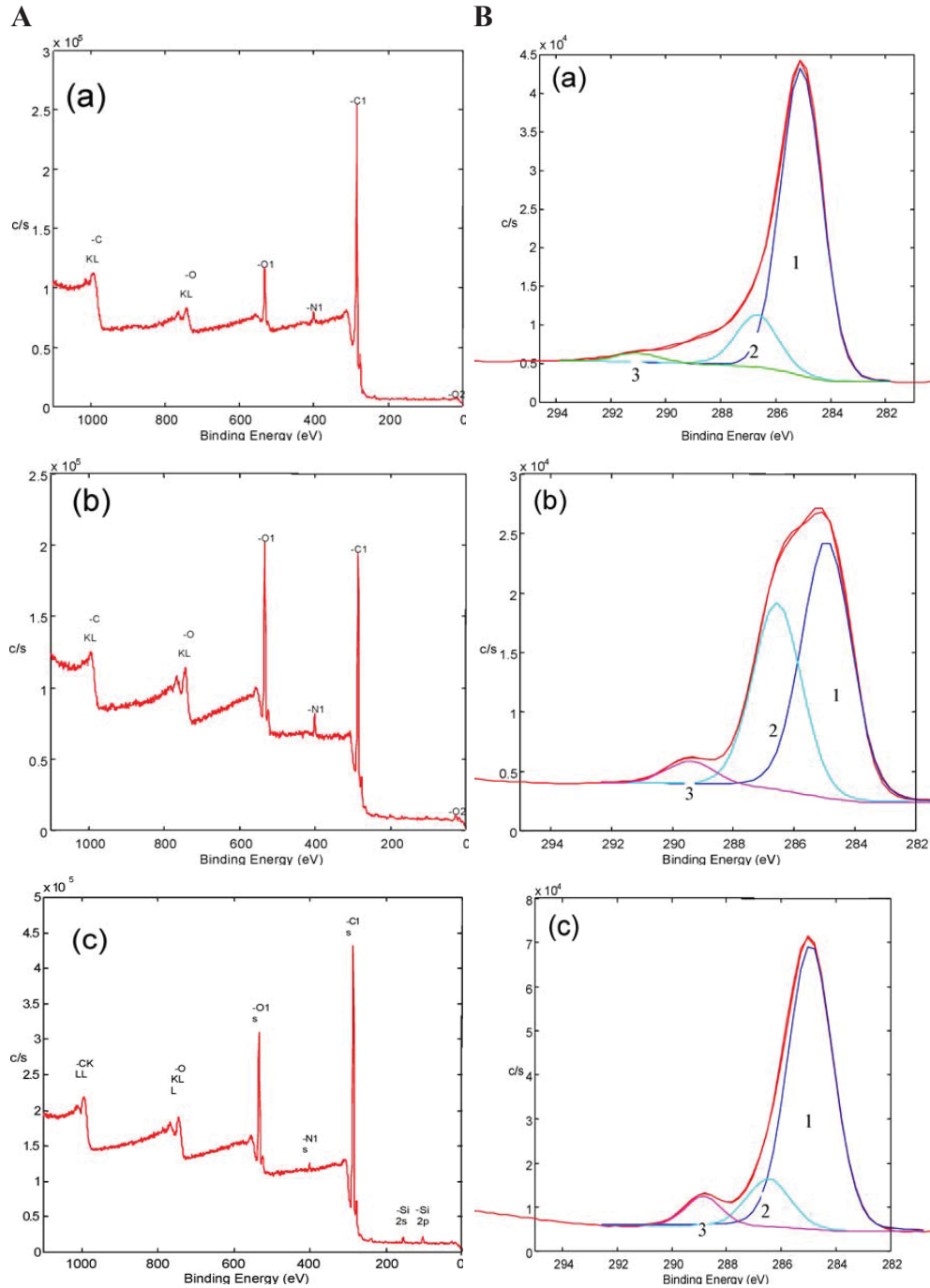


Fig.5. A – XPS wide scan spectra of carbon fibers: (a) untreated, (b) air-oxidation treated, and (c) gamma-irradiated; B – XPS core level spectra of C1s region of carbon fibers: (a) untreated, (b) air-oxidation treated, and (c) gamma-irradiated (graphitic carbon (C–C, peak 1), hydroxyl group (OH, peak 2), and the carboxyl group (COOH, peak 3) were found) [18].

since all carbons and oxygens present in C–O bonds exhibit very minor differences in core level BE. To detect a carboxylic group  $-(COOH)$ , the reaction under precise conditions with 2,2,2-trifluoroethanol will produce  $CO(OCH_2CF_3)$  groups on the polymer surface. Thus, the carboxylic function is directly titrated by recording the XPS F1s peak, with distinctive advantages, due to the three fluorine atoms replacing one carboxylic group, the F1s cross-section being larger than the C1s one and the peak area of F1s unambiguously attributed to the specific reaction. The detection limit in this case is well below 0.2% groups per carbon atom.

- Surface modification of polymers. XPS is conducted without special preparation of samples, but is carried out in an ultra-high vacuum environment ( $10^{-9}$  Torr). Thus, biomaterial samples must be in a dry state. Some instruments using a liquid nitrogen-cooled stage permit the analysis of frozen hydrated samples. Although X-rays can penetrate materials to depths of 1  $\mu\text{m}$  or more, XPS provides information about the outermost 5–75  $\text{\AA}$  layer, because photoelectrons originating deeper in the sample lose energy in inelastic collision and/or do not have sufficient energy to be emitted from the sample. The depth of analysis is typically 3 to 10 nm, with a lateral resolution of 150  $\mu\text{m}$ . This is used in applications which include: liquid/solid interfaces, impurity segregation, polymer coatings, transfer films, thin film chemistry. Using the XPS technique, it was observed [18] that the composites reinforced with the gamma-irradiated carbon fibers showed higher interfacial adhesion and thus better flexural and shear properties than the composites reinforced with air-treated fibers (Fig.5). It was suggested that the higher content of carboxyl groups observed on the surface of the gamma-irradiated carbon fibers was most likely responsible for the stronger fiber-matrix bonding.
- Neutron reflectivity is ideally suited for determining the structure of the interface between immiscible polymers. It is also used for solving of other polymer problems, such as: surface separation in polymer blends, polymer adsorption from solution, the study of grafted polymer layers, and surface-driven lamellar ordering in block copolymers [19]. Neutron reflectometry coupled with ellipsometry shows details of the thin film morphology and structure at solid/liquid interfaces and is used in the study of biocompatible thin films.

Optical and scanning force microscopies (SFM) covers atomic force microscopy (AFM), scanning tunneling microscopy (STM) and near-field scanning optical microscopy (NSOM). Polymer science has benefited from the continuous development of scanning probe microscopy (SPM) techniques, which allow full characterization of polymer films at the nanoscale: such as film morphology, mechanical properties (*i.e.* stiffness, deformability, adhesion, and friction), electrical and thermal properties (*i.e.* glass-transition, melting and crystallization temperatures), and so forth. The capability of studying surface reorganizations in real time through *in situ* experiments makes SPM a valuable and ver-

satellite tool, able to give insight on the physicochemical properties of polymer films with unprecedented detail.

Topographical features of polymer surfaces are easily revealed and material contrasts can be established either by differences in the mechanical properties of the materials or by selective removal of one of the two phases using a selective solvent. A comparison of different optical and SPM surface analysis techniques is provided in Figs.6A and B.

One of the most common techniques used for measurement of the surface morphology and other mechanical properties is atomic force microscopy. Using this technique, an oscillating small spring-like cantilever with a sharp tip fixed on its free end examines the sample surface. Tip radius of curvature can be as small as a size of one atom and ranges up to  $1\ \mu\text{m}$ . The deflections of the cantilever are determined by the detector and the forces between tip and surface are estimated. These forces can be as small as  $10^{-9}$ - $10^{-10}$  N.

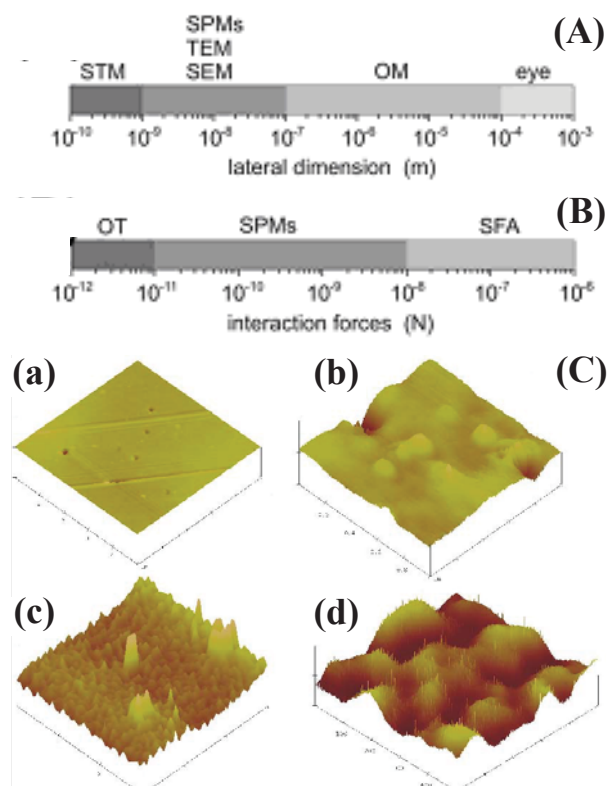


Fig.6. (A) Comparison of different SPMs with surface imaging techniques classified according to measurable size (STM – scanning tunneling microscopy, SPMs – scanning probe microscopies, TEM – transmission electron spectroscopy, SEM – scanning electron microscopy, and OM – optical microscopy). (B) Surface force techniques are classified according to the strength of interactions. (C) AFM images of (a) pristine poly(methyl methacrylate) (PMMA), irradiated with fluencies of (b)  $4 \times 10^{14}$ , (c)  $4 \times 10^{15}$  and (d)  $1 \times 10^{16}$  e/cm<sup>2</sup> [20].



Changes in surface morphology of pristine PMMA samples after irradiation are shown in Fig.6C. The tapping mode of the AFM (TM-AFM) showed the hills of the nano size surrounded by crater type features in all irradiated samples. It was found that the root-mean-square (RMS) surface roughness of the samples increased from 2.7 to 5.6 nm when the electron fluency correspondingly increased from  $2 \times 10^{14}$  to  $1 \times 10^{16}$  e/cm<sup>2</sup> [20].

Care must be taken when topographical features are imaged by tapping mode AFM in that different phases have very different mechanical properties.

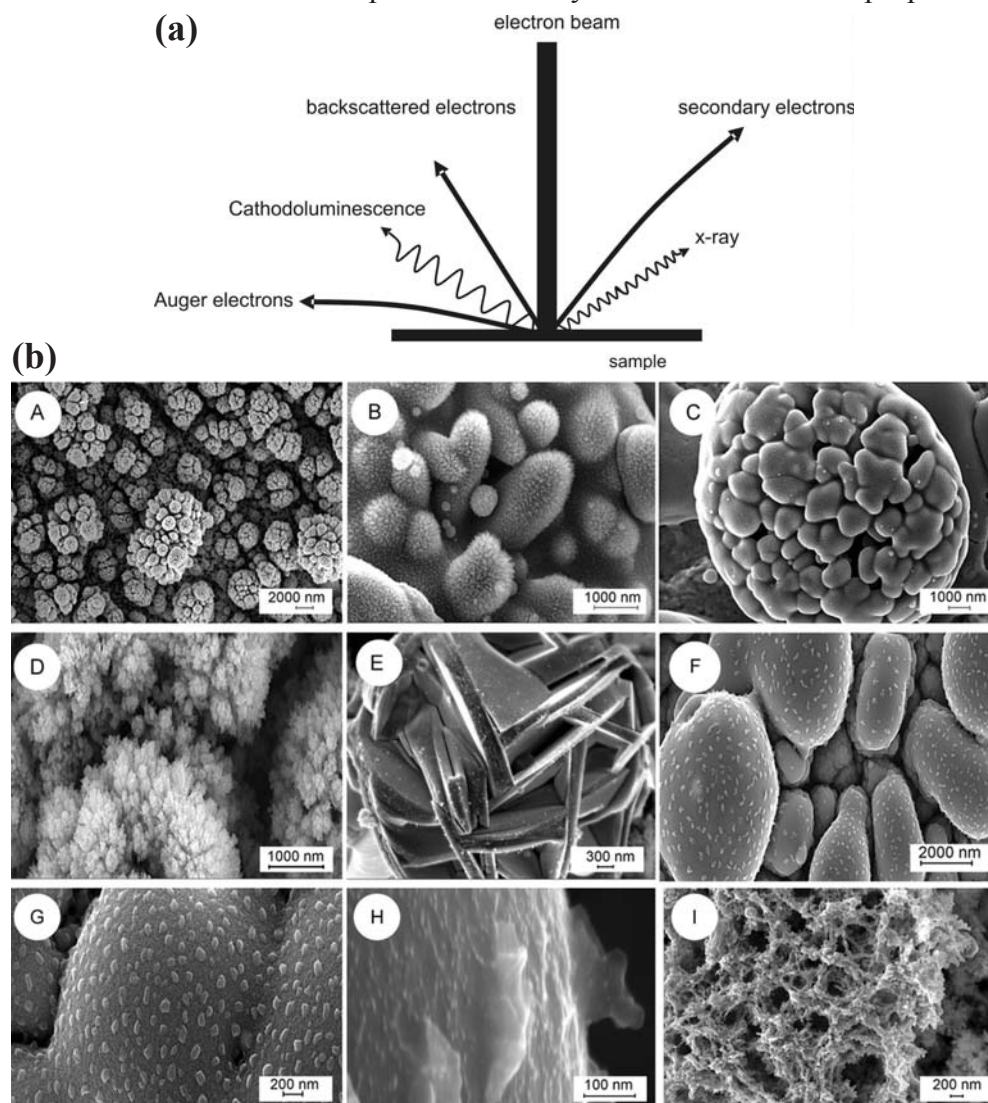


Fig.7. (a) Emissions produced in a performing SEM analysis. (b) SEM images of MoO<sub>3</sub> nanostructures: (A-E) deposited in the pin-to-pin electrode configuration, (F-H) deposited in the pin-to-plate electrode configuration, (I) porous networks of MoO<sub>3</sub> deposited in the pin-to-plate configuration [23].



Differences in tip indentation into the surface may interfere with the real topographical features and the interpretation of the apparent surface topography becomes difficult [21].

Biodegradable polycaprolactone (PCL)/poly-l-lactide (PLLA)/coconut fiber composites were irradiated using an electron beam accelerator to an absorbed dose of 100 kGy [22]. Regions with different elasticity indicated the presence of fibers on the surface of the composites. The spherical structure sizes decreased on the surface of the composites.

The different kinds of signals and images that are produced using a scanning electron microscope are shown in Fig.7 and described in Table 3. For the successful examination of a specimen by SEM, the sample must be carefully prepared. Embedded liquids and gases in the sample must be removed by appropriate treatment (*e.g.* storage at elevated temperatures or in vacuum). Surfaces of non-conductive samples should be sputtered with a thin conductive layer. For these reasons noble metals like gold, palladium and platinum serve as the typical coating materials. In the case of X-ray analysis, the sample is analyzed according to its composition and should not be coated with the above-mentioned metals but with carbon. Many thin polymer films, though non-conductive in bulk, can be imaged without coverage by a conducting material (metals, carbon, *etc.*).

Table 3. Emissions related to SEM operation and features to examine/obtained information.

Emission/signal	Features to examine/obtained information
Secondary electrons	Topographical observation of surface, potential contrast, crystalline structure, magnetic contrast
Backscattered electrons	Compositional observation of surface, magnetic contrast
X-ray	Element analysis of specimen
Transmitted electrons	Internal structure
Cathodoluminescence	Internal characteristics

Scanning can also be done in the transmission mode to circumvent problems associated with transmission electron microscopy (TEM), such as poor contrast [24]. X-rays produce an energy dispersive X-ray (EDX) spectrum that can identify the elements in the imaged area. Some SEM capabilities are: large depth of field, 3 nm resolution (100 000x), digital imaging and archiving, electron channeling, *etc.* Spatial resolution of a few nanometers along all three spatial axes has been demonstrated. Element analysis using the EDX spectrum and the wavelength dispersive X-ray (WDX) spectrum is mainly applied to inorganic materials. These methods are only rarely used in the field of polymer science, but find applications such as the characterization of inorganic-organic hybrid surfaces.

Standard SEM is conducted in a high vacuum environment, which prevents biological samples from being investigated in their native state. Newer instruments, called environmental scanning electron microscopes (ESEM), allow visualization of at least partially hydrated samples.

Contact angle measurement is the most common method for determining the free surface energy of solid surfaces. This provides data on surface energetics, roughness, heterogeneity, as well as on surface dynamics, allowing one to monitor the behavior at solid-liquid interfaces. There are two main methods of solid surface tension measurements: (i) the contact angle (the most frequently used and most accessible technique) and (ii) the inverse gas chromatography method.

The contact angle method is sensitive to the topmost few angstroms, due to the forces involved in the wetting process. A liquid drop deposited on a solid surface will modify its shape under the pressure of different surface/interfacial tensions until equilibrium is reached. In the thermodynamics of wetting, the minimization of the free energy of the system imposes one and only one value for the contact angle. A liquid drop on a solid surface can have many different stable angles, continuously varying between two relatively well reproducible values, the maximum being usually called the advancing angle and the minimum – the receding angle. The difference between these two values is known as the contact angle hysteresis. From the contact angle hysteresis, the fraction of polar and non-polar surface segments can be estimated. One of the main disadvantages of the contact angle method is that only ideal surfaces (rigid, homogeneous, and smooth) can be used to measure the true equilibrium contact angle for a liquid-solid interface.

Young's equation describes a state of stable equilibrium, being valuable for an ideal surface:

$$\gamma_{sv} - \gamma_{sl} = \gamma_{lv} \cos \theta \quad (2)$$

where:  $\gamma_{sv}$  – the surface tension of the solid (s) in equilibrium with the saturated vapor (v) of the liquid (l),  $\gamma_{sl}$  – the interfacial tension between the solid and the liquid, and  $\gamma_{lv}$  – the surface tension of the liquid in equilibrium with its saturated vapor,  $\theta$  – the equilibrium contact angle between a drop of liquid deposited on a solid and the respective surface, as shown in Fig.8.

Surface tension has the dimension of force per unit length or of energy per unit area. The two are equivalent, but when referring to energy per unit of area, it is common to use the term surface energy, which is the more general term in that it applies also to solids.

The wetting liquid must be a neutral one, so that neither physical nor chemical interactions with the solid occur.

The surface tension may be considered as a sum of independent terms. The geometrical mean could describe polar and dispersion interactions, by the following equation:

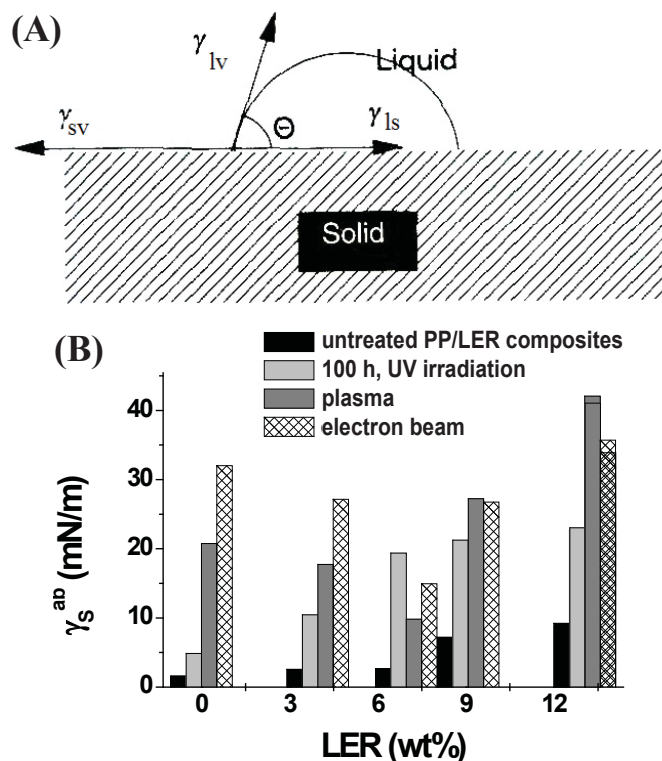


Fig.8. (A) Interfacial tensions at the contact between three media and (B) acid-base component of the free surface energy vs. epoxidized lignin (LER) content for isotactic polypropylene (IPP)-based composites, exposed to different irradiation sources [25].

$$\gamma_{sl} = \gamma_s + \gamma_l - 2(\gamma_s^d \gamma_l^d)^{1/2} - 2(\gamma_s^p \gamma_l^p)^{1/2} \quad (3)$$

where:  $\gamma_s$  and  $\gamma_l$  – the total surface tension of the solid (s) and of liquid (l), respectively;  $\gamma_s^d$  (or  $\gamma_s^{LW}$ ) and  $\gamma_l^d$  (or  $\gamma_l^{LW}$ ) – dispersive components of surface tension of solid and liquid, respectively;  $\gamma_s^p$  and  $\gamma_l^p$  – polar components of surface tension of solid and liquid, respectively.

Also the harmonic mean method [26] may be used where the dispersion ( $I_d$ , noted also with  $\gamma_s^{LW}$ ,  $\gamma_l^{LW}$ , respectively – Eq. (5)) and the polar ( $I_p$ ) terms are substituted by:

$$I_d = 2(\gamma_l^d \gamma_s^d) / (\gamma_l^d + \gamma_s^d) \quad \text{and} \quad I_p = 2(\gamma_l^p \gamma_s^p) / (\gamma_l^p + \gamma_s^p) \quad (4)$$

In both cases the two components of the free surface energy of solid can be determined using at least two liquids of having known surface tensions and of different polarities (generally, water and methylene iodide).

The asymmetric acid-base parts of a bipolar system can be split into separate surface energy components: the acid ( $\gamma^+$ ) and the basic ( $\gamma^-$ ) components of the surface energy.  $\gamma^+$  is the contribution of the proton donor (electron acceptor), while  $\gamma^-$  that of the proton acceptor (electron donor).

With these considerations, the Young-Good-Girifalco-Fowkes equation becomes:

$$\gamma_1(1 + \cos \theta) = 2 \left[ (\gamma_s^{LW} \gamma_1^{LW})^{1/2} + (\gamma_s^+ \gamma_1^-)^{1/2} + (\gamma_s^- \gamma_1^+)^{1/2} \right] \quad (5)$$

The interfacial tension  $\gamma_{ij}^{ab}$  between the i and j phases can be expressed as:

$$\gamma_{ij}^{ab} = 2 \left[ (\gamma_i^+ \gamma_j^-)^{1/2} + (\gamma_j^+ \gamma_i^-)^{1/2} - (\gamma_i^- \gamma_j^+)^{1/2} - (\gamma_i^+ \gamma_j^-)^{1/2} \right]$$

or

$$\gamma_{ij}^{ab} = 2 \left[ (\gamma_i^+)^{1/2} - (\gamma_j^+)^{1/2} \right] \left[ (\gamma_i^-)^{1/2} - (\gamma_j^-)^{1/2} \right] \quad (6)$$

where  $\gamma_{i(or,j)}^-$  and  $\gamma_{i(or,j)}^+$  are the contributions of the proton acceptor (electron donor) and proton donor (electron acceptor) to the polar component of the free surface energy, respectively.

Two methods may be applied for evaluation of the different components of the free surface energy of a system using Eq. (5). The first one requires three polar liquids having known surface tension components to be deposited on the respective surface in order to obtain the corresponding contact angles. The second method requires one non-polar liquid for finding  $\gamma^{LW}$  and two other polar liquids. The acid-base component of free surface energy increased due to any treatment of IPP/LER blends whether by ultraviolet (UV) irradiation, plasma exposure or electron beam bombardment (Fig.8B). This acid-base component increases regardless of the treatment applied [25].

Four commonly used methods for contact angle (surface tension) measurement are: (i) the sessile drop, (ii) the tilting plate, (iii) the captive bubble, and (iv) the Wilhelmy plate technique.

Work of adhesion ( $W_a$ ) is defined as the work required when separating liquid and solid phases, or the negative free energy associated with the adhesion of the solid and liquid phases. It is used to express the strength of the interaction between the two phases and it is given by the Young-Dupré equation as:

$$W_a = \gamma (1 + \cos \theta) \quad (7)$$

Wetting tension, ( $\tau$ ) a measure of the force/length or strength of the wetting interaction, is defined as:

$$\tau = \gamma_{lv} \cos \theta \quad (8)$$

It is also referred to as adhesion tension or work of wetting.

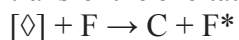
Chemiluminescence (CL) is the emission of light (luminescence) as the result of a chemical reaction. Such chemical reactions produce energy in sufficient amount to induce the transition of an electron from its ground state to an excited electronic state. This electronic transition is often accompanied by vibrational and rotational changes in the molecule. Given reactants **A** and **B**, with an excited intermediate, the following describes such reactions:



Chemiluminescence is defined as the emission of ultraviolet, visible or infrared radiation from a molecule or atom as the result of the transition of an

electronically excited state. When the reaction occurs in a living system or it is derived from one, the process is called bioluminescence (BL).

Sometimes, the excited product [ $\diamond$ ] is an ineffective emitter, but it can transfer the excitation energy to an efficient fluorophore (F) added to the system:



↓

F + Light

The emission is then identical with the fluorescence of the fluorophore F. Analytically, the CL reactions are attractive since they: (i) have excellent sensitivity and wide detection limits due to the absence of source noise and scatter; (ii) are sometimes highly selective due to the limited number of available reactions; (iii) are simple, robust and rely on inexpensive instrumentation suitable to both batch or flow analytical techniques. CL methods have been used in drug analysis, in sea water analysis or in determining antioxidant activity in natural and synthetic products [27]. They have been widely used for sensitive detection and measurement of reactive oxygen species involved in the oxidative processes. Oxidative changes in food are important in terms of nutritional quality, flavor, odor, spoilage, and potential toxicity resulting from ingestion of oxidation reaction products. Oxidative stress is an important hypothesis in explaining the genesis of several pathologies, including cancer, atherosclerosis, aging or Alzheimer's disease. Several components of food and natural products (phenolic compounds, vitamins, *etc.*) have protective functions in the aforementioned pathologies. This seems to be due to their ability to scavenge reactive oxygen.

The radiation degradation of polypropylene was studied by measuring the chemiluminescence from gamma-irradiated samples. The chemiluminescence emitted by recombination of peroxy radicals was found to increase with the increasing dose, thus reflecting the degree of oxidation of the polymer. The degradation of PP is attributed mainly to oxidation, since the degradation of PP irradiated in air was markedly greater than that in vacuum. The degree of oxidation was found to be very high at the surface of the films where oxygen can diffuse during irradiation and was decreased sharply with increasing depth from the surface. The degradation during PP storage after irradiation was estimated by the decay curves of the chemiluminescence [28].

Chemiluminescence analysis was used to determine the oxidation layer formed by electron beam irradiation of polypropylene for medical devices. Oxidation was found to occur near the surface of the film where the diffusion of oxygen was greater [29].

Ethylene-vinyl acetate (EVA) copolymers undergo thermal degradation by the macromolecular breakdown after irradiation to a dose of 12 kGy, as shown in Fig.9 [30]. The oxidation induction period, *i.e.* time until the CL intensity reached its maximum value, decreased with increasing treatment temperature.

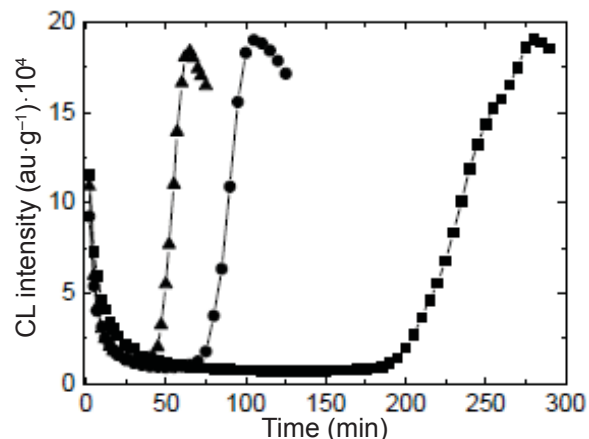


Fig.9. The time dependence of CL intensity with the treatment temperature for irradiated EVA copolymer at 12 kGy. Measurement temperatures: (■) 200°C, (●) 210°C, (▲) 220°C [30].

Combining several of the surface property methods is recommended in order to achieve reliable results.

### 3. METHODOLOGIES FOR THE CHARACTERIZATION OF SOME BULK PROPERTIES

Industry uses ionizing radiation to modify the properties of polymers for use in many areas. The irradiation of polymers can lead to crosslinking and/or chain scissioning reactions, depending on the chemical structure of the polymer and the irradiation conditions. Generally, crosslinking results in an increase in tensile strength, hardness, softening temperature, solvent resistance, abrasion resistance, dimensional stability, and a decrease in elongation at break [31, 32].

Chain scissioning most often leads to reduced tensile strength, hardness and softening temperature, and increased solubility and elongation. Crosslinking and scissioning occur simultaneously in a polymer during irradiation and the overall change in properties depends on which process predominates.

For a given polymer, the irradiation conditions that most affect the relative amounts of crosslinking and chain scissioning are the dose rate, and the presence of oxygen, additives and solvents and the irradiation temperature.

Several important bulk properties of polymers are affected by irradiation: chemical composition and structure, average molecular weight, solubility, mechanical properties (Young's modulus, tensile, impact, hardness, fatigue, flexural modulus, *etc.*), electric and optical properties, crystallinity, transition temperatures (mainly glass transition related to Vicat softening point and



brittleness temperature), gas permeability across a polymer film or a membrane, water absorption, melt viscosity and rheological properties, polymer stability under aging, biological factors, temperature and UV resistance, weathering (environmental stress), *etc.* Descriptions of many methods used to determine the bulk properties of irradiated materials can be found in Refs. [33, 34].

Several important properties of polymers are related to their bulk morphology. Methods used to evaluate surface morphology have been discussed above. In food packaging, the crystallinity, the glass transition temperature and barrier properties are of interest including migration phenomena from packaging materials to food, as possible with the use of nanoparticles. Methods to characterize these properties are described below.

### 3.1. GLASS TRANSITION TEMPERATURE

The glass transition temperature ( $T_g$ ) is the temperature at which several physical characteristics of polymers change, such as: specific heat capacity ( $c_p$ ), coefficient of thermal expansion, mechanical modulus, dielectric constant.

The glass-liquid transition or glass transition is the reversible transition in amorphous materials (or in amorphous regions within semicrystalline materials) from a hard and relatively brittle “glassy” state into a molten or rubber-like state, as the temperature is increased. The reverse transition, achieved by cooling a liquid into the glass state, is called vitrification. The temperature at which the transition in a material changes between a glassy, hard state to a rubbery or liquid state is called the glass transition temperature.

Three techniques are generally used for determining  $T_g$ :

- differential scanning calorimetry (DSC),
- thermomechanical analysis (TMA),
- dynamic mechanical analysis (DMA).

In each of these techniques, a change in a sample is determined as a function of temperature.

Differential scanning calorimetry is a traditional and widely used technique with many polymeric materials. Depending on the equipment capability, DSC can be used for a wide range of thermoplastic and thermoset polymers. The glass transition, as illustrated in Fig. 10, appears as a step in the DSC curve and shows the change of the specific heat capacity ( $c_p$ ) from the glassy/vitreous to the rubbery phase.

$T_g$  can be calculated by using a half-height technique in the transition region. This procedure is described in the ISO standard 11357-2:1999 [35].

For a given polymer, the glass transition temperature depends on polymer morphology that includes molecular weight, branching, crystallinity, the amount and type of additives and traces of solvents/water. For irradiated polymers,  $T_g$  also depends on dose [36, 37].



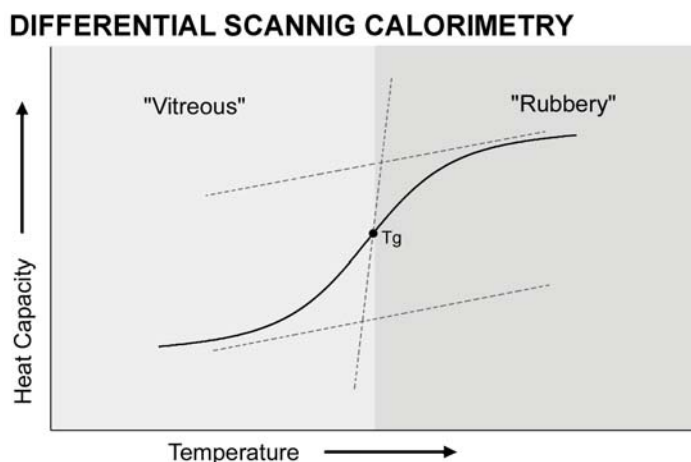


Fig.10. Typical DSC curve.

Carswell-Pomerantz *et al.* [38] evaluated the glass transition of fluoro-polyimide (FPI) samples at different gamma irradiation doses. Before irradiation, the  $T_g$  of FPI was 280°C. After irradiation to 600 and 1800 kGy, the  $T_g$  of FPI increased to 295 and 310°C, respectively. These temperature changes in  $T_g$  were attributed to crosslinking of the FPI, which hinders molecular mobility. The higher  $T_g$  also indicates an increase in crosslinked density. Different properties can be obtained if the polymer is irradiated below or above its glass transition temperature, as it was reported by Sun and Zhong [39] in their study of tacticity changes of isotactic poly(methyl methacrylate) (PMMA) and syndiotactic PMMA samples.

### 3.2. DEGREE OF CRYSTALLINITY

The crystallization of polymers is a more complicated process than the crystallization of low molecular weight materials. This is related to the wide distribution of chain lengths of macromolecules, the high interfacial free energy associated with the basal plane of the crystallites and to the difficulty in extracting ordered sequences of macromolecules of sufficient length from the disordered melt in a finite or reasonable time. The crystallization of long chain, higher molecular weight molecules will only occur during long cool down cycles, which gives rise to a complex arrangement of molecules with a polycrystalline character and to the coexistence of crystalline and amorphous components.

The degree of crystallinity of a polymer is the relative amount of crystalline and amorphous components and can be expressed on either a volume or mass basis. The degree of crystallinity depends on the crystallization conditions, the degree of polymer branching, polymer side chain bulkiness, and the regu-

larity of molecular configuration. The dependence on irradiation dose should be taken into account when examining irradiated polymers. In particular, the degree of crystallinity will increase in following order:

- slow cooling more than fast cooling (this allows time for diffusion to occur and for polymer chains or segments to align),
- linear more than branched more than crosslinked polymers,
- isotactic and syndiotactic more than atactic polymers,
- simple repeat units more than bulky side chains in repeat units.

For polymers that crystallize, the crystallinity influences many properties of some manufactured products (Table 4). More crystalline polymers tend to be mechanically stronger and more resistant to chemical attack and to softening by heat.

Table 4. Effect of increase in crystallinity on different polymer properties [40]. ↑ represents increase and ↓ represents decrease (with increasing crystallinity).

S/N	Property	Effect of crystallinity
1	Density	↑
2	Tensile strength	↑
3	Clarity	↓
4	Permeability	↓
5	Opacity	↑
6	Compressive strength	↑
7	Impact strength	↓
8	Tear resistance	↓
9	Toughness	↓
10	Ductility	↓
11	Ultimate elongation	↓

The degree of crystallinity can be determined using several methodologies based on density measurement, X-ray diffraction, and the determination of melting enthalpy. All these methodologies are based on a two-phase model, having crystalline and amorphous phases.

Using volume ( $x_v$ ) and mass ( $x_m$ ), the degree of crystallinity can be determined from density measurements using the following equations:

$$x_v = [(\rho - \rho_a)/(\rho_c - \rho_a)] \times 100 \quad (10a)$$

$$x_m = [\rho_c(\rho - \rho_a)/\rho(\rho_c - \rho_a)] \times 100 \quad (10b)$$

where  $\rho$ ,  $\rho_a$  and  $\rho_c$  are the densities of the sample, of the same material in amorphous phase and in the crystalline phase, respectively.

A typical wide-angle X-ray diffraction (WAXD) curve for a semicrystalline polymer has sharp diffraction peaks resulting from the crystalline phase

of a sample material and a broad diffuse halo corresponding to the amorphous phase of that material. The areas under the “amorphous” halo and the “crystalline” peaks are used to determine degree of crystallinity:

$$\% \text{ Crystallinity} = \frac{\text{Area under crystalline peaks}}{\text{Total area under all peaks}} \times 100\% \quad (11)$$

The degree of crystallinity can also be obtained measuring the melting enthalpy of the sample and comparing its value with the melting enthalpy of the polymer having nearly 100% crystallinity. The usual procedure in determining the degree of crystallinity by DSC involves drawing an arbitrary linear baseline from the onset of melting to the last trace of crystallinity and determining the enthalpy of fusion from the area under this endotherm, as illustrated in Fig. 11. The degree of crystallinity is then defined as:

$$\% \text{ Crystallinity} = [\Delta H_f / \Delta H_f^\circ] \times 100 \quad (12)$$

where  $\Delta H_f$  is the enthalpy of fusion measured at the melting point ( $T_m$ ), and  $\Delta H_f^\circ$  is the enthalpy of fusion of the 100% crystalline polymer measured at the equilibrium melting point ( $T_m^\circ$ ).

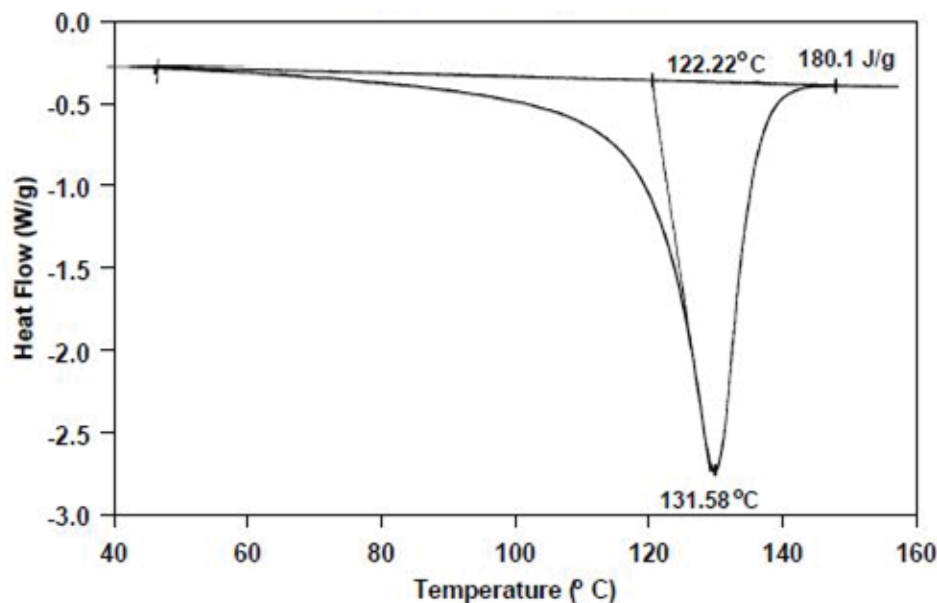


Fig. 11. Melting endotherm for a polyethylene sample after heating.

The relative degree of crosslinking and scissioning in polymers when irradiated are effected by the degree of crystallinity of the polymer. Since crosslinking usually takes place in the amorphous phase, increased crystallinity in a polymer reduces its ability to crosslink [41]. At the same time, irradiation may alter the crystallinity in polymers. Increased crosslinking reduces the ability of a polymer to recrystallize because the three-dimensional polymer network produced by crosslinking inhibits crystallite formation. Under certain irradiation

tion conditions some crystalline polymers can undergo radiation-induced chain scissioning followed by recrystallization which stops the degradation process and generates a sample with increased crystallinity.

Table 5. Crystallinity by X-ray diffraction in PLA nanocomposites containing clay (Dellite D67G) nanoparticles before and after irradiation to 1 and 10 kGy [41].

Sample	Xc [%]
PLA/D67G 1%	–
PLA/D67G 1%_1 kGy	2
PLA/D67G 1%_10 kGy	3
PLA/D67G 3%	4
PLA/D67G 3%_1 kGy	6
PLA/D67G 3%_10 kGy	5
PLA/D67G 5%	8
PLA/D67G 5%_1 kGy	9
PLA/D67G 5%_10 kGy	7

The admixture of clay nanoparticles and the influence of irradiation on the crystallinity of poly(lactic acid) (PLA)-based nanocomposites was investigated using WAXD [42, 43]. Unmodified PLA remains amorphous after irradiation to the doses of 1 and 10 kGy [41, 42]. For the nanocomposites containing clay nanoparticles, however, the X-ray diffraction patterns showed the formation of a crystalline phase. Some crystals of the  $\alpha$ -form were observed in PLA nanocomposite containing 1 wt% of clay (Dellite D67G) and the crystallinity increased for nanocomposites containing 3 and 5 wt% of Dellite D67G. The values of crystallinity are reported in Table 5.

### 3.3. BARRIER PROPERTIES

Barrier properties are of importance in food packaging because they control the ability of a package to preserve its contents from the deleterious effects of gases, aromas, humidity, *etc.* UNI (UNI 10534 12/94) defines the limits of permeability associated with low and high barrier properties (Table 6).

Permeability (P) is defined as the quantity of gas passing through a unit surface area, of given thickness, under a partial and unitary difference of pressure in the unit of time. The permeability of plastic films is a function of several polymer characteristics (chemical type, morphology, and crystallinity), of environmental factors (temperature, relative humidity, difference of pressure), of thickness and geometry of the packaging, and the kind and size of permeant

Table 6. Barrier properties range.

Barrier	Permeability [ $\text{cm}^3/(\text{m}^2 \cdot 24 \text{ h}) \cdot (\text{cm}/\text{bar})$ ]
Very high	< 0.5
High	0.5-3.0
Medium	3.1-30
Low	31-150
Very low	> 150

gas molecules or particles. Permeability is also influenced by the amount, distribution, and size of such particles because the presence of these particles affects the path of gas molecules.

Barrier properties are linked to the diffusion parameters. Fick's laws are used to study the diffusion parameters of polymers. Fick's first law is an empirical expression. It states that the flux (mass per unit time per unit area) traveling through a material is equal to  $-D$  (the diffusion coefficient or diffusivity) times the concentration gradient ( $dc/dx$ ) with respect to the distance traveled ( $x$ ) [44]:

$$j = -D (dc/dx) \quad (13)$$

Fick's first law applies strictly to neutral, non-interacting particles only. For other situations, the coefficient  $D$  is not a constant.

Fick's law in terms of permeability ( $P$ ) and the pressure gradient ( $dp/dx$ ) can be written as:

$$j = -D (dc/dx) = -P (dp/dx) \quad (14)$$

Converting  $dp/dx$  gradient into actual values, the following equation can be obtained for the permeability:

$$P = Q \times x / A \times (p_1 - p_2) \quad (15)$$

where:  $Q$  – the fluid flow rate defined as the quantity of fluid or gas ( $\text{O}_2$ ,  $\text{N}_2$ ,  $\text{CO}_2$ , water vapor) passing through a unit area in the unit of time with the

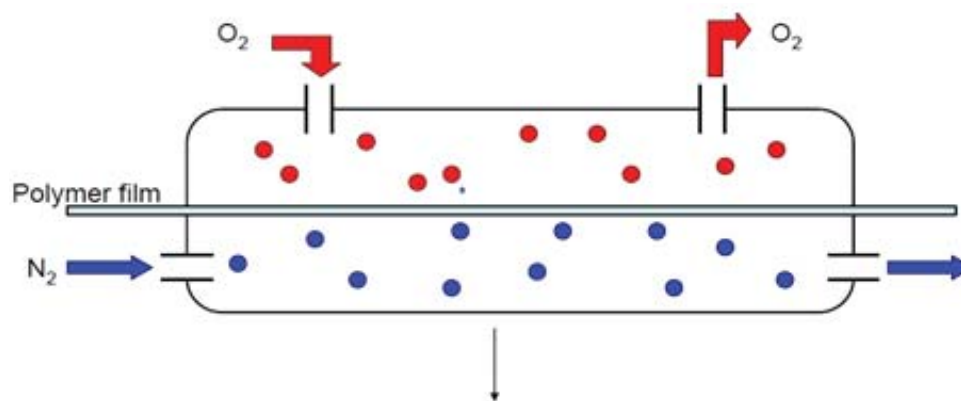


Fig.12. Operating principle of a gas permeability tester.

difference of pressure ( $p_1 - p_2$ ),  $A$  – the sample surface, and  $x$  – the sample thickness. This equation can be used to calculate  $P$  from the measurements performed using a permeability testing apparatus, as shown in Fig.12. The permeability testing apparatus consists of a double diffusion chamber with the test film inserted between the two chambers. For the evaluation of oxygen permeability, oxygen enters into the upper chamber, while anhydrous nitrogen enters the bottom one as a carrier gas. The chambers are conditioned at 23°C. As the oxygen gas permeates through the specimen (polymer film) into the carrier gas, it is transported to the coulometric detector where it creates an electric current which is proportional to the number of oxygen atoms flowing into the detector.

This test is performed in accordance with ASTM D3985 which determines the amount of oxygen that passes through the surface (50 cm<sup>2</sup>) of the film of a given thickness, in a certain time (24 h), with precise relative humidity conditions (0%) and temperature (23°C).

### **3.4. PARTICLES MIGRATION**

Packaging protects foodstuff from spoilage. However, the transfer of chemicals from packaging to food may have a negative impact on the quality and safety of the food since no food contact material is completely inert and there is a need to ensure the safety of such materials. The main consumer demand is that the packaging should not be a source of contamination in the food.

Any mass transfer from an external source into food by particle migration is important when developing a new packaging material for the market. Such migration may impact on food in two ways: (i) causes safety problems related to the migration of harmful substances and (ii) causes quality problems related to the migration of substances which impart taint or odor. To overcome some of these problems, polymer-based food packaging is irradiated. When a polymer packaging material is subjected to irradiation not only the migration of the typical additives must be taken into consideration but also the radiolytic products (RPs) generated during the irradiation process. The RPs from some commonly used polymers consist of low molecular weight aldehydes, acids and olefins. In the case on packaging based on nanomaterials the migration of the nanoparticles must be also assessed.

Typical additives for plastics are: stabilizers, UV absorbers, preservatives, optical brighteners, foaming agents, release agents, antioxidants, plasticizers, lubricants, emulsifiers, fillers, flame retardants, impact modifiers.

The migration ability of particles increases with temperature and decreases with the dimension of the migrating substance.

Migration tests are usually performed by using food simulants that are intended to mimic the migration properties of different categories of foods. This

methodology was introduced in the early 1980s along with the rules for using simulants. The basics for migration tests are reported in the following European Community (EC) documents:

- 82/711/EEC – Basic rules for testing migration,
- 93/8/EEC – 1st amendment,
- 97/48/EEC – 2nd amendment,
- 85/572/EEC List of simulants,
- 10/2011/EU List of simulants.

According to the regulations the following steps need to be performed:

- selection of simulant which is based on a food type (Table 7),
- selection of the exposure type,
- selection of the exposure time and temperature.

Table 7. Types of simulants used for food packaging testing.

Simulant	Abbreviation	Food
Ethanol 10% (v/v) in water	Simulant A	Aqueous foods
Acetic acid 3% (w/v) in water	Simulant B	Acidic foods (< pH 4.5)
Ethanol 20% (v/v) in water	Simulant C	Alcoholic foods (< 20% alcohol)
Ethanol 50% (v/v)	Simulant D1	Foods with an alcohol content of above 20% and for oil in water emulsions
Vegetable oil	Simulant D2	Foods with an alcohol content of above 20% and for oil in water emulsions
Modified poly(phenylene oxide)s, particle size – 60-80 mesh, pore size – 200 nm	Simulant E	Dry foods

The migration models in different food stuffs are set in EC regulations and are normally quoted from migration tests using the following values: 600 cm<sup>2</sup> of print, 1 kg of food, 10 days at 40°C.

Migration tests may be performed in four ways depending on the form and the dimensions of the material or article to be tested:

- by using a migration test cell,
- by preparation of a pouch,
- by total immersion,
- by article filling.

For most of the samples the total immersion method is used: the sample (1 dm<sup>2</sup>) is immersed in the simulant.

For total immersion tests, different procedures have been adopted according to the type of the selected food simulant. In the case of aqueous simulants,



the overall migration is calculated by determining the mass (M) of the residue after evaporation of the water in the food simulant.

For fatty food the determinations, the overall migration into vegetable oil is more complicated. The value of the overall migration is measured by determining the weight loss from the sample. Taking into account that the sample might have absorbed components of the fatty simulant during contact, the weight loss of the sample must be corrected for the amount of absorbed fat [45].

The effect of irradiation on the migration behavior of particles from packaging to food is reported in the literature. Zygoura *et al.* [46] compared the effect of irradiation type and dose on the specific migration behavior of poly(vinyl chloride) (PVC) films. The migration levels of a plasticizer (acetyl tributyl citrate – ATBC) from PVC into the European Union (EU) aqueous food simulants (distilled water, 3% w/v acetic acid and 10% v/v ethanol) after PVC films were irradiated to 5, 15 and 25 kGy doses using an electron beam or gamma rays (Co-60 unit) were studied. The electron beam irradiated films had significantly higher ATBC migration as compared to gamma treatment, although for both types of ionizing radiation the values defining ATBC migration into the aqueous food simulants were far below the EU limits (1 mg·kg<sup>-1</sup> body weight). Because of these results, it was concluded that irradiated PVC cling films may be used in contact with aqueous foodstuffs.

Jeon *et al.* [47] evaluated the effect of gamma irradiation on the migration levels of two antioxidants, tris-(2,4-di-tert-butylphenyl) phosphite (Irgafos 168) and octadecyl-3-(3,5-di-tert-butyl-4-hydroxyphenyl) propionate (Irganox 1076), on linear low density polyethylene (LLDPE) films treated at doses ranging from 0 to 200 kGy. The migration of Irgafos 168 from a LLDPE pouch into food simulants, distilled water, acetic acid (4 ml/100 ml distilled water) or ethanol (20 ml/100 ml distilled water), was not detected at dose levels up to 200 kGy while Irganox 1076 was detected in a decreasing mode with increasing doses.

#### **4. CONCLUSIONS AND FUTURE TRENDS**

The use of the main methods to study the changes in the surface and bulk properties of irradiated polymers was presented, emphasizing the advantages and limitations of each method. As instrumentation and theory continue to develop, methods will also improve to facilitate the understanding of the effects of radiation on polymer structure and morphology which subsequently influence the final properties of products.

### Acknowledgments

The authors acknowledge the financial support given by the International Atomic Energy Agency (IAEA) by research contract No. 17689 (RC-17689-R0).

### REFERENCES

- [1]. Vasile, C., & Pascu, M.C. (2007). *Surface properties of polymers*. Kerala, India: Research Signpost.
- [2]. StJohn, H.A.W., Gengenbach, T.R., Hartley, P.G., & Grisser, H.J. (2003). Surface analysis of polymers. In D.J. O'Connor, B.A. Sexton & R.St.C. Smart (Eds.), *Surface analysis methods in materials science* (pp. 519-553). Berlin, Heidelberg: Springer. (Springer Series in Surface Sciences 23).
- [3]. Murray, K.A., Kennedy, J.E., McEvoy, B., Vrain, O., Ryan, D., Cowman, R., & Higginbotham, C.L. (2013). Characterisation of the surface and structural properties of gamma ray and electron beam irradiated low density polyethylene. *International Journal of Material Science (IJMSCI)*, 3(1), 1-8.
- [4]. Klauber, C., & Smart, R.St.C. (2003). Solid surfaces, their structure and composition. In D.J. O'Connor, B.A. Sexton & R.St.C. Smart (Eds.), *Surface analysis methods in materials science* (pp. 3-81). Berlin, Heidelberg: Springer. (Springer Series in Surface Sciences 23).
- [5]. Israelachvili, J.N. (1992). *Intermolecular and surface forces*. London: Academic Press.
- [6]. Garbassi, F., Morra, M., & Occhiello, E. (1994, 1998). *Polymer surfaces. From physics to technology*. Chichester: John Wiley & Sons.
- [7]. Ratner, B.D. (1988). *Surface characterization of biomaterials*. Amsterdam: Elsevier Science Publishers.
- [8]. Goessl, A., Jung, L., Bowen-Pope, D., & Hoffman, A.S. (2002). Affinity patterning of biomaterials using plasma gas discharge. In *Radiation synthesis and modification of polymers for biomedical applications. Final results of a co-ordinated research project, 1996-2000*. Vienna: IAEA. (IAEA-TECDOC-1324).
- [9]. Onyiriuka, E.C. (1993). The effects of high-energy radiation on the surface chemistry of polystyrene: A mechanistic study. *J. Appl. Polym. Sci.*, 47(12), 2187-2194.
- [10]. Jenkins, S. (2016, January). *Principle of SIMS (Secondary Ion Mass Spectrometry)*. Retrieved January 14, 2016, from [http://www.lpdlabservices.co.uk/analytical\\_techniques/surface\\_analysis/sims/index.php](http://www.lpdlabservices.co.uk/analytical_techniques/surface_analysis/sims/index.php).
- [11]. Leggett, G.J., & Vickerman, J.C. (1992). An empirical model for ion formation from polymer surfaces during analysis by secondary-ion mass spectrometry. *Int. J. Mass Spectrom. Ion Processes*, 122, 281-319.
- [12]. SurfaceSpectra Ltd. (2012). Retrieved January 14, 2016, from <http://www.SurfaceSpectra.com/>.
- [13]. Parparita, E., Zaharescu, T., Darie, R.N., & Vasile, C. (2015). Biomass effect on gamma-irradiation behavior of some polypropylene biocomposites. *Ind. Eng. Chem. Res.*, 54(8), 2404-2413.

- [14]. Gupta, R., Kumar, V., Goyal, P.K., Kumar, S., Kalsi, P.C., & Lata Goyal, S. (2011). Effect of  $\gamma$ -irradiation on thermal stability of CR-39 polymer. *Adv. Appl. Sci. Res.*, 2(1), 248-254. Retrieved January 14, 2016, from <http://pelagiaresearch-library.com/advances-in-applied-science/vol2-iss1/AASR-2011-2-1-248-254.pdf>.
- [15]. Briggs, D., & Seah, M.P. (1983). *Practical surface analysis*. New York: John Wiley.
- [16]. Andrade, L.D. (1985). *Surface and interfacial aspects of biomedical polymers*. New York: Plenum Press.
- [17]. Beamson, G., & Briggs, D. (1992). *High resolution XPS of organic polymers: The Scienta ESCA300 Database*. Chichester: Wiley.
- [18]. Bradley, R.H., Ling, X., & Sutherland, I. (1993). An investigation of carbon fibre surface chemistry and reactivity based on XPS and surface free energy. *Carbon*, 31(7), 1115-1120.
- [19]. Russell, T.P. (1990). X-ray and neutron reflectivity for the investigation of polymers. *Mater. Sci. Rep.*, 5, 171-271.
- [20]. Nathawat, R., Kumar, A., & Vijay, Y.K. (2007). Morphological changes of electron-beam irradiated PMMA surface. In C. Petit-Jean-Genaz (Ed.), *Particle accelerator. Proceedings, 22nd Conference, PAC'07, Albuquerque, USA, June 25-29, 2007* (pp. 2745-2747). Piscataway, USA: IEEE.
- [21]. Stoleru (Paslaru), E., Tsekov, Y., Kotsilkova, R., Ivanov, E., & Vasile, C. (2015). Mechanical behavior at nano-scale of chitosan-coated PE surface. *J. Appl. Polym. Sci.*, 132(31), 42344.
- [22]. Kodama, Y., Oishi, A., Nagasawa, N., Nakayama, K., Tamada, M., & Machado, L.D.B. (2013). Atomic force microscopy investigation of electron beam (EB) irradiated composites based on biodegradable polymers and coconut fiber. *Nukleonika*, 58(4), 459-468.
- [23]. Pai, D.Z., Ostrikov, K., Kumar, S., Lacoste, D.A., Levchenko, I., & Laux, C.O. (2013). Energy efficiency in nanoscale synthesis using nanosecond plasmas. *Sci. Rep.*, 3, 1221. DOI: 10.1038/srep01221.
- [24]. Laurer, J.H., & Winey, K.I. (1998). Direct imaging of ionic aggregates in Zn-neutralized poly(ethylene-co-methacrylic acid) copolymers. *Macromolecules*, 31(25), 9106-9108.
- [25]. Pascu, M., Vasile, C., & Gheorghiu, M. (2003). Modification of polymer blend properties by argon plasma/electron beam treatment: surface properties. *Mater. Chem. Phys.*, 80, 2, 548-554.
- [26]. Wu, S. (1971). Calculation of interfacial tension in polymer systems. *J. Polym. Sci. C*, 34, 19-30.
- [27]. Jimenez A.M., & Navas, M.J. (2002). Chemiluminescence methods (present and future). *Grasas y Aceites*, 53(1), 64-75.
- [28]. Ishigaki, I., & Yoshii, F. (1992). Radiation effects on polymer materials in radiation sterilization of medical supplies. *Int. J. Radiat. Appl. Instrum. C: Radiat. Phys. Chem.*, 39(6), 527-533.
- [29]. Yoshii, F., Sasaki, T., Makuuchi, K., & Tamura, N. (1986). Durability of radiation-sterilized polymers III. Oxidation layer determined by chemiluminescence. *J. Appl. Polym. Sci.*, 31(5), 1343-1350.

- [30]. Jipa, S., Zaharescu, T., Senescu, R., & Kappel, W. (2007). Chemiluminescence study on the endurance of ethylenevinylacetate (EVA) under radiation and thermal degradation. *J. Opt. Adv. Mater.*, 9(6), 1623-1625.
- [31]. Bruce, M.B., & Davis, M.V. (1981). *Radiation effects on organic materials in nuclear plants*. Electric Power Research Institute. (Final Report EPRI NP-2129).
- [32]. Drobny, J.G. (2012). *Ionizing radiation and polymers principles, technology and applications*. Oxford: Elsevier.
- [33]. Sperling, L.H. (1992). *Introduction to physical polymer science* (2nd ed.). New York: Wiley-Interscience.
- [34]. van Krevelen, D.W. (1990). *Properties of polymers* (3rd ed.). Amsterdam: Elsevier Science.
- [35]. ISO. (1999). *Plastics – Differential scanning calorimetry (DSC) – Part 2: Determination of glass transition temperature*. ISO 11357-2:1999. Retrieved January 14, 2016, from [http://www.iso.org/iso/iso\\_catalogue/catalogue\\_ics/catalogue\\_detail\\_ics.htm?csnumber=25545](http://www.iso.org/iso/iso_catalogue/catalogue_ics/catalogue_detail_ics.htm?csnumber=25545).
- [36]. Davenas, J., Stevenson I., Celette, N., Cambon, S., Gardette, J.L., & Rivaton, A. (2002). Stability of polymers under ionising radiation: The many faces of radiation interactions with polymers. *Nucl. Instrum. Meth. B.*, 191(1), 653-661.
- [37]. Sasuga, T., & Hagiwara, M. (1986). Mechanical relaxation of crystalline poly(aryl-ether-ether-ketone) (PEEK) and influence of electron beam irradiation. *Polymer*, 27, 821-826.
- [38]. Carswell-Pomerantz, T., Babanalbandi, A., Dong, L., Hill, D.J.T., Perera, M. C.S., Pomery, P.J., Saadat, G., & Whittaker, A.K. (1999). Changes in molecular structure and properties of irradiated polymers of different compositions. ESR and NMR study. In *Stability and stabilization of polymers under irradiation*. Vienna: IAEA. (IAEA-TECDOC-1062). Retrieved January 14, 2016, from [www-pub.iaea.org/mtcd/publications/pdf/te\\_1062\\_prn.pdf](http://www-pub.iaea.org/mtcd/publications/pdf/te_1062_prn.pdf).
- [39]. Zhong, X., & Sun, J. (1999). Studies on radiation stability of polymers. In *Stability and stabilization of polymers under irradiation*. Vienna: IAEA. (IAEA-TECDOC-1062). Retrieved January 14, 2016, from [www-Pub.Iaea.Org/Mtcd/Publications/Pdf/Te\\_1062\\_Prn.Pdf](http://www-Pub.Iaea.Org/Mtcd/Publications/Pdf/Te_1062_Prn.Pdf).
- [40]. Selke, S., Culter, J., & Hernandez, R. (2004). *Plastics packaging: Properties, processing, applications, and regulations* (2nd ed.). Munich: Hanser Publications.
- [41]. Drobny, J.G. (2010). *Radiation technology for polymers* (2nd ed.). Boca Raton: CRC Press.
- [42]. Salvatore, M., Marra, A., Duraccio, D., Shayanfar, S., Pillai, S.D., Cimmino, S., & Silvestre, C. (2016). Effect of electron beam irradiation on the properties of polylactic acid/montmorillonite nanocomposites for food packaging applications. *J. Appl. Polym. Sci.*, 133, 42219.
- [43]. Shayanfar, S., Smith, B., Pillai, S., Duraccio, D., & Silvestre, C. (2014). Bioplastics and MAP to enhance sustainable packaging and food quality: The role of electron beam (eBeam) technology as a platform technology for enhancing packaging materials and food quality. IFT'14, New Orleans, USA.
- [44]. Zeman, S., & Kubik, L. (2007). Permeability of polymeric packaging materials technical sciences. *Techn. Sc.*, 10. DOI 10.2478/v10022-007-0004-6.

- [45]. Simoneau, C. (2009). *Guidelines on testing conditions for articles in contact with foodstuffs*. European Communities. (JRC Scientific and Technical Reports). Retrieved January 14, 2016, from [http://www.iss.it/binary/moca/cont/guidelines\\_test\\_conditions.pdf](http://www.iss.it/binary/moca/cont/guidelines_test_conditions.pdf).
- [46]. Zygoura, P., Paleologos, E., & Kontominas, M. (2011). Effect of ionizing radiation treatment on the specific migration characteristics of packaging – food simulant combinations: Effect of type and dose of radiation. *Food Addit. Contam.*, 28, 686-694.
- [47]. Jeon, D.H., Park, G.Y., Kwak, I.S., Lee, K.H., & Park, H.J. (2007). Antioxidants and their migration into food simulants on irradiated LLDPE film. *LWT*, 40(1), 151-156.